

Thermodynamic properties of two-component fermionic atoms trapped in a two-dimensional optical lattice

Kensuke Inaba and Makoto Yamashita

*NTT Basic Research Laboratories, NTT Corporation, Atsugi 243-0198, Japan and
CREST, JST, Chiyoda-ku, Tokyo 102-0075, Japan*

(Dated: November 6, 2018)

We study the finite temperature properties of two-component fermionic atoms trapped in a two-dimensional optical lattice. We apply the self-energy functional approach to the two-dimensional Hubbard model with a harmonic trapping potential, and systematically investigate the thermodynamic properties of this system. We find that entropy and grand potential provide evidence of a crossover between the Mott insulating and metallic phases at certain temperatures. In addition, we find that entropy exhibits a cusp-like anomaly at lower temperatures, suggesting a second or higher order antiferromagnetic transition. We estimate the antiferromagnetic transition temperatures, and clarify how the trapping potential affects this magnetic transition.

PACS numbers: 03.75.Ss, 05.30.Fk, 67.85.Lm, 75.30.Kz

I. INTRODUCTION

Ultracold atoms in an optical lattice created by interfering laser beams are bridging the gap between theoretical and experimental studies in the field of condensed matter physics. We can control the depth, interstice and dimension of the lattice by manipulating lasers, and the interaction between ultracold atoms by using the Feshbach resonance [1]. This high degree of controllability allows us to simulate correlated many-body systems experimentally [2–5]. Theoretically, it has been pointed out that this system can be regarded as a realization of the Hubbard model, which is one of the most fundamental models including the many-body effects [6–8]. In fact, various phenomena described by this model have been successfully demonstrated in experiments [9–15].

The first experimental progress was reported as an observation of the quantum phase transition of bosonic ^{87}Rb atoms between a superfluid and a Mott insulator in an optical lattice [9]. As regards the fermionic atoms, the Fermi surface and its topological change were observed in the fermionic ^{40}K optical lattice system, suggesting a metal to band-insulator transition [10]. Recently, by combining numerical and experimental studies, it was clarified that a Mott transition was realized in ^{40}K optical lattice systems [11, 12]. In these reports, the Hubbard model with a trapping potential was analyzed by using a local density approximation with the dynamical mean-field approach (LDA+DMFT)[12] and a zero-tunneling limit calculation [11]. The effects of the trapping potential, which is an important characteristic of ultracold atoms in an optical lattice, have been properly taken into account in addition to those of the correlations. However, these calculations present certain difficulties in terms of investigating magnetic transitions. The observation of the magnetic ordered phase in the optical lattice system is a major concern for condensed matter physicists, because it could provide ways to elucidate the nature of high T_c superconductors [16]. By using the recently developed real-space dynamical mean-field theory (R-DMFT) [17–

20], it has been pointed out that an antiferromagnetic (AF) ordered phase is stable in the Hubbard model with a trapping potential at zero temperature [18]. This naturally motivates us to undertake a detailed study of both the magnetic transition and the Mott transition at finite temperatures using a reliable numerical method.

For this purpose, we investigate the two-component Fermi-Hubbard model in a two-dimensional (2D) optical lattice with a harmonic trapping potential at finite temperatures. We make use of the self-energy functional approach (SFA), which has been successfully applied to homogeneous Hubbard-type lattice models [21–24]. We demonstrate that this method can properly take account of the effects of the trapping potential in addition to those of strong correlations and thermal fluctuations. SFA further provides us with important thermodynamic quantities such as grand potential and entropy. We find that both Mott and AF transitions can be characterized by the behavior of these thermodynamic quantities. The AF transition temperatures of the present model are systematically examined by varying the temperature, interaction strengths and curvatures of the harmonic trapping potential.

This paper is organized as follows. In Sec. II, we introduce the two-component Fermi-Hubbard model on a 2D optical lattice with a harmonic trapping potential. In Sec. III, we briefly outline the application of SFA to the present system. In Sec. IV, we discuss the finite temperature properties of the Mott insulating region. In Sec. V, we discuss how the AF ordered region is realized in the system, and estimate the AF transition temperatures. In Sec. VI, we briefly summarize this paper.

II. MODEL

In this paper, we investigate the two-component Hubbard model on a 2D lattice with a trapping potential that we assume to be harmonic. The Hamiltonian of this

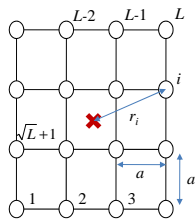


FIG. 1: (Color online) A schematic diagram of the 2D lattice, where the cross is the center of the harmonic trapping potential, L is the total number of sites, a is the lattice distance, and r_i is the distance between the center of the trap and the i th site. The numbers written in the top right of the lattice sites correspond to the site indices.

model is given by $\mathcal{H} = \mathcal{H}_t + \mathcal{H}_U$,

$$\mathcal{H}_t = J \sum_{\langle i,j \rangle} \sum_{\sigma} c_{i\sigma}^{\dagger} c_{j\sigma} + \sum_i \sum_{\sigma} (V_t r_i^2 - \mu) n_{i\sigma}, \quad (1)$$

$$\mathcal{H}_U = \sum_i U n_{i\uparrow} n_{i\downarrow}, \quad (2)$$

where $c_{i\sigma}^{\dagger} (c_{i\sigma})$ creates (annihilates) a fermionic atom with pseudospin $\sigma (= \uparrow, \downarrow)$ at the i th site, and $n_{i\sigma} = c_{i\sigma}^{\dagger} c_{i\sigma}$. Here, we describe the nearest-neighbor hopping integral as J , the curvature of a harmonic trapping potential as V_t , the chemical potential as μ , and the interaction strength between two atoms with different pseudospins as U . For simplicity, we define the site index i as shown in Fig. 1, where L is the number of sites, a is the lattice distance, and r_i is the distance between the i th site and the center of the trap. It is useful to introduce the parameter matrix \mathbf{t} , which characterizes the non-interacting Hamiltonian \mathcal{H}_t as

$$[\mathbf{t}]_{ij} = \begin{cases} V_t r_i^2 & \text{if } i = j \\ J & \text{if the } i\text{th site neighbors the } j\text{th site} \\ 0 & \text{otherwise} \end{cases} \quad (3)$$

We define the scales of length and energy in the following way such that the calculated results do not depend on the details of the parameters, *e.g.* L , a , V_t , and μ . We introduce the characteristic trap length $r_t = \sqrt{N_{\sigma}}/\sqrt{\pi}a$, which corresponds to the radius of a non-interacting atomic cloud in the zero-tunneling limit, where N_{σ} is the total number of atoms with pseudospin σ . The distance r_i is rescaled by this r_t as $r_{SC} \equiv r_i/r_t$. We also introduce the bandwidth $W = 8J$ as a scale of energy. We consider the characteristic trap energy $E_t = V_t r_t^2$, which corresponds to the Fermi energy in the zero-tunneling limit [12]. In addition to E_t/W , we consider two parameters: the temperature T/W and the interaction strength U/W .

Before concluding this section, we summarize the physical quantities calculated in this paper. The rescaled cloud size, which characterizes the Mott and band in-

ulating phases [12], is defined as,

$$R_{SC} = \langle r \rangle / r_t, \quad (4)$$

$$\langle r \rangle = \sqrt{\sum_i r_i^2 N_i / \sqrt{N_{\text{tot}}}}, \quad (5)$$

where $N_i = \sum_{\sigma} \langle n_{i\sigma} \rangle$ is the number of atoms at the i th site, and $N_{\text{tot}} = \sum_i N_i$ is the total number of atoms. To discuss the magnetic ordered phase, we calculate the magnetization $M_i = \langle n_{i\uparrow} \rangle - \langle n_{i\downarrow} \rangle$. We also investigate thermodynamic quantities: grand potential Ω and entropy $S = -\partial\Omega/\partial T$, which are sensitive to both the Mott transition and the AF transition.

III. METHOD

The thermodynamic properties of the present system are studied with the self-energy functional approach (SFA) [21–23], which is based on the Luttinger-Ward variational method [25]. It has been pointed out that SFA allows us to undertake an efficient investigation of the finite temperature properties of homogeneous Hubbard-type lattice systems, for instance, the infinite-dimensional Hubbard model [21, 22] and also the 2D Hubbard model [24], taking account of the effects of strong correlations. We extend this method to deal with inhomogeneous systems. Here, we explain an application of this SFA to the Hubbard model with a trapping potential.

First, we begin by briefly explaining the general framework of the SFA. According to the Luttinger-Ward functional approach [25], the grand potential Ω of a Hubbard-type system described by the Hamiltonian $\mathcal{H} = \mathcal{H}_t + \mathcal{H}_U$ is written as,

$$\Omega[\Sigma] = F[\Sigma] + \text{Tr} \ln[(\mathbf{G}_0^{-1} - \Sigma)^{-1}], \quad (6)$$

where $F[\Sigma]$ is the Legendre transformation of the Luttinger-Ward potential, Σ is the self-energy, and $\mathbf{G}_0 = (\omega - \mu - \mathbf{t})^{-1}$ is the non-interacting Green function. Here, we use the notation $\text{Tr} \mathbf{A} = T \sum_{\omega_n, i} [\mathbf{A}]_{ii}(i\omega_n)$, where $\omega_n = (2n + 1)\pi T$ is the Matsubara frequency. Under the condition $\partial\Omega[\Sigma]/\partial\Sigma = 0$, we obtain the physical Green function \mathbf{G} that satisfies the Dyson equation $\mathbf{G}^{-1} = \mathbf{G}_0^{-1} - \Sigma$. In general, the functional $F[\Sigma]$ is not known explicitly, which prevents an evaluation of $\Omega[\Sigma]$. However, the potential $F[\Sigma]$ does not depend on the details of the non-interacting Hamiltonian \mathcal{H}_t as long as the shape of the interaction term \mathcal{H}_U remains unchanged [21]. This allows us to introduce a reference system that has a Hamiltonian with the same interaction term as that of the original system. This reference Hamiltonian is explicitly given by $\mathcal{H}^{\text{ref}} = \mathcal{H}_{\mathbf{t}'} + \mathcal{H}_U$ with the *variational* parameter matrix \mathbf{t}' . The grand potential of the reference system Ω^{ref} is then written as,

$$\Omega^{\text{ref}}[\Sigma] = F[\Sigma] + \text{Tr} \ln[(\mathbf{G}'_0^{-1} - \Sigma)^{-1}], \quad (7)$$

where $\mathbf{G}'_0 = (\omega - \mu - \mathbf{t}')^{-1}$. By subtracting Eq. (7) from Eq. (6), we can rewrite the grand potential of the original system as a function of the self-energy for the reference system Σ^{ref} :

$$\begin{aligned} \Omega[\Sigma^{\text{ref}}] &= \Omega^{\text{ref}} + \text{Tr} \ln [(\omega + \mu - \mathbf{t} - \Sigma^{\text{ref}})^{-1}] \\ &\quad - \text{Tr} \ln [(\omega + \mu - \mathbf{t}' - \Sigma^{\text{ref}})^{-1}]. \end{aligned} \quad (8)$$

A reference system with an optimized parameter matrix \mathbf{t}' satisfying the condition

$$\partial\Omega[\Sigma^{\text{ref}}]/\partial\mathbf{t}' = 0, \quad (9)$$

gives us an appropriate self-energy Σ^{ref} , Green function $\mathbf{G} = (\omega - \mu - \mathbf{t} - \Sigma^{\text{ref}})^{-1}$ and grand potential $\Omega[\Sigma^{\text{ref}}]$, which approximately describe the physical quantities of the original system.

An application of the SFA to the Hubbard model with a trapping potential is achieved as follows. The simplest reference system with which to investigate the present model is L -sets of two-site Anderson impurity models [22]. Here, the i th impurity site, corresponding to the i th site of the original lattice, is connected to the i th non-interacting atomic bath. The Hamiltonian of this reference system is given by the form: $\mathcal{H}^{\text{ref}} = \sum_i \mathcal{H}_i^{\text{ref}}$, and

$$\begin{aligned} \mathcal{H}_i^{\text{ref}} &= \sum_{\sigma} (\epsilon_i + \sigma h_i) c_{i\sigma}^{\dagger} c_{i\sigma} \\ &\quad + \sum_{\sigma} \left(V_{i\sigma} c_{i\sigma}^{\dagger} a_{i\sigma} + H.c. \right) + U n_{i\uparrow} n_{i\downarrow}, \end{aligned} \quad (10)$$

where $a_{i\sigma}^{\dagger} (a_{i\sigma})$ creates (annihilates) an atom with pseudospin σ at the i th atomic bath. The variational parameter $V_{i\sigma}$ is the hybridization of the impurity and the atomic bath, ϵ_i is the effective potential, and h_i is the effective magnetic field. Here, we briefly explain the role of variational parameters ϵ_i , h_i and $V_{i\sigma}$. By optimizing an effective potential ϵ_i under the condition $\partial\Omega/\partial\epsilon_i = 0$, the number of atoms N_i is properly adjusted [23]. We can discuss the stability of magnetic ordered phases via the condition $\partial\Omega/\partial h_i = 0$ [23, 26, 27]. The hybridization $V_{i\sigma}$ effectively describes the hopping integral between the i th site and adjacent sites in the original lattice; therefore, we can also discuss the Mott transition via the conditions $\partial\Omega/\partial V_{i\sigma} = 0$ [21, 22]. Details of the role of the atomic bath with the hybridization term will be discussed in appendix A.

By employing exact diagonalization, we can easily obtain the grand potential Ω_i^{ref} and the self-energy $\Sigma_{i\sigma}^{\text{ref}}$ of the i th reference system. Now, the grand potential of the original system is given by,

$$\Omega = \sum_i \Omega_i^{\text{ref}} - \sum_{\sigma} \text{Tr} \ln \mathbf{G}_{\sigma}^{\text{ref}} + \sum_{\sigma} \text{Tr} \ln \mathbf{G}_{\sigma}, \quad (11)$$

$$\mathbf{G}_{\sigma} = (i\omega_n + \mu - \mathbf{t} - \Sigma_{\sigma}^{\text{ref}})^{-1}, \quad (12)$$

$$\mathbf{G}_{\sigma}^{\text{ref}} = (\mathbf{G}_{0\sigma}^{\text{ref}-1} - \Sigma_{\sigma}^{\text{ref}})^{-1}, \quad (13)$$

where $[\mathbf{G}_{0\sigma}^{\text{ref}}]_{ij} = \delta_{ij}/(i\omega_n - \epsilon_i - \sigma h_i - V_{i\sigma}^2/i\omega_n)$, and $[\Sigma_{\sigma}^{\text{ref}}]_{ij} = \delta_{ij} \Sigma_{i\sigma}^{\text{ref}}$. The variational condition (9) is rewritten as,

$$T \sum_{i\omega_n} ([\mathbf{G}_{\sigma}]_{ii} - [\mathbf{G}_{\sigma}^{\text{ref}}]_{ii}) \frac{\partial \Sigma_{i\sigma}^{\text{ref}}}{\partial \mathbf{t}'_i} = 0, \quad (14)$$

where we denote the variational parameter sets as $\mathbf{t}'_i = \{\epsilon_i, h_i, V_{i\uparrow}, V_{i\downarrow}\}$. Note that $[\mathbf{G}_{\sigma}^{\text{ref}}]_{ii}$ and $\partial \Sigma_{i\sigma}^{\text{ref}}/\partial \mathbf{t}'_i$ depend only on one parameter set \mathbf{t}'_i . In contrast, $[\mathbf{G}_{\sigma}]_{ii}$ depends on all of the elements of the variational parameter matrix \mathbf{t}' , and we have to solve an equation of the $4L$ th degree. It is still difficult for the large size system to solve equation (14) and to optimize the variational parameter matrix \mathbf{t}' . To avoid this difficulty, we introduce another parameter matrix \mathbf{t}^* and local Green functions as $G_{i\sigma}^{\text{loc}}(\mathbf{t}', \mathbf{t}^*) = (G_{i\sigma}^{\text{cav}-1}(\mathbf{t}^*) - \Sigma_{i\sigma}^{\text{ref}}(\mathbf{t}'))^{-1}$, where $G_{i\sigma}^{\text{cav}}(\mathbf{t}^*) = \left(\Sigma_{i\sigma}^{\text{ref}}(\mathbf{t}^*) + [\mathbf{G}_{\sigma}(\mathbf{t}^*)]_{ii}^{-1} \right)^{-1}$. We replace $[\mathbf{G}_{\sigma}]_{ii}$ in equation (14) with $G_{i\sigma}^{\text{loc}}$ considering the additional self-consistent condition $[\mathbf{G}_{\sigma}]_{ii} = G_{i\sigma}^{\text{loc}}$. If \mathbf{t}^* is given, the variational condition (14) is finally rewritten as,

$$\frac{\partial}{\partial \mathbf{t}'_i} \left(\Omega_i^{\text{ref}} - T \sum_{\sigma\omega_n} \ln G_{i\sigma}^{\text{ref}} + T \sum_{\sigma\omega_n} \ln G_{i\sigma}^{\text{loc}} \right) = 0. \quad (15)$$

We note that the equation of the $4L$ th degree is decomposed into independent L -sets of the 4th degree. Now, we choose \mathbf{t}^* as a parameter matrix satisfying this new condition (15), and repeatedly solve this variational problem until \mathbf{t}^* converges (at the same time, the self-consistent condition $[\mathbf{G}_{\sigma}]_{ii} = G_{i\sigma}^{\text{loc}}$ is satisfied). In summary, we self-consistently solve independent L -sets of easily solvable SFA problems instead of a huge problem with the $4L$ th degree.

The procedure mentioned above can be extended to any other inhomogeneous systems. In addition, if we deal with the attractively interacting systems, we can straightforwardly extend the scope of this method to the s -wave superfluid phase by adding the term, $\Delta_i c_{i\uparrow}^{\dagger} c_{i\downarrow}^{\dagger} + H.c.$, to the reference Hamiltonian (10), where Δ_i is a variational parameter corresponding to the superfluid order parameter. Furthermore, the SFA has been successfully applied to multi-component Fermi systems [28], where it has been suggested that novel quantum phase transitions could be observed [29–32]. Promising candidates for such systems are fermionic ^{173}Yb atoms [14] and/or ^6Li atoms [33, 34].

Now, we describe briefly how to calculate the physical quantities. It is possible to evaluate various quantities denoted in the previous section by means of the Green function $\mathbf{G}(\omega)$, the grand potential Ω , and its derivatives. For instance, the total number of atoms is obtained by the relations: $N_{\text{tot}} = \partial\Omega/\partial\mu$ or $N_{\text{tot}} = \text{Tr} \mathbf{G}$. Note that the variational condition $\partial\Omega/\partial\mathbf{t}' = 0$ guarantees that these two relations are equivalent to each other

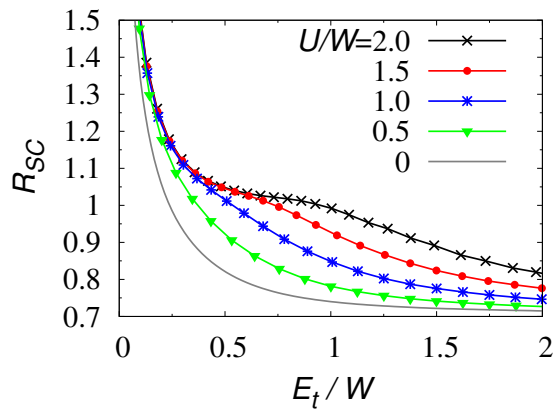


FIG. 2: (Color online) Rescaled cloud size R_{SC} as a function of E_t/W for different U/W at $T/W = 0.1$.

[35]. In addition, the SFA allows us to calculate quantities in momentum space, *e.g.* experimentally observed time of flight images. We can also calculate angle resolved photo emission spectra using the present scheme, which is closely related to a recent observation by the JILA group in Ref. [36]. However, it is beyond our current scope to investigate these quantities in momentum space.

We close this section with few comments on the superiority of the SFA to other related numerical approaches. The zero-tunneling limit calculation and LDA+DMFT present certain difficulties when we discuss quantum phase transitions accompanied by spontaneous symmetry breaking. Although R-DMFT can be applied to the magnetic ordered phase [18] and the superfluid phase [19, 20], it is difficult to investigate the finite temperature properties systematically and precisely with this method. In contrast, the SFA provides comprehensive ways to investigate various quantum phase transitions at finite temperatures. Moreover, this method allows us to calculate various useful quantities observed experimentally.

IV. MOTT INSULATING PHASE

In this section, we investigate the finite temperature properties of the 2D Hubbard model with a harmonic trapping potential. In particular, we focus on the behavior of the thermodynamic quantities of this model at certain temperatures, where the Mott insulating region is observed.

First, to discuss the validity of our method, we calculate the rescaled cloud size R_{SC} which was previously evaluated for the three dimensional (3D) model by the LDA+DMFT approach in Ref. [12]. Figure 2 shows R_{SC} as a function of E_t/W for different U/W values, where the temperature is fixed at $T/W = 0.1$. When the interaction strength is small ($U/W = 0, 0.5$ and 1.0), R_{SC} decreases rapidly in the weakly trapped re-

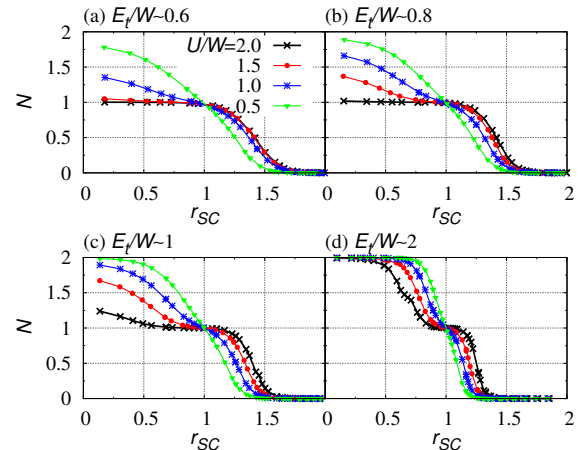


FIG. 3: (Color online) Density profiles of atomic cloud, *i.e.* the number of atoms N_i as a function of the rescaled distance r_{SC} for several fixed values of E_t/W : (a) 0.6, (b) 0.8, (c) 1.0 and (d) 2.0. The interaction strength is varied from $U/W = 0.5$ to $U/W = 2.0$. The temperature is fixed at $T/W = 0.1$.

gion $E_t/W < 1$, while it changes little in the strongly trapped region $E_t/W > 1$. It should be noted that, in the strongly trapped limit $E_t/W \gg 1$, R_{SC} finally converges to $1/\sqrt{2} \sim 0.7$, which corresponds to the cloud size of non-interacting atoms without tunneling. This indicates that most of the atoms except for those around the site $r_i \sim r_t$ become inactive; in other words, the band-insulating like state appears [12]. On the other hand, for large U/W values of 1.5 and 2, the R_{SC} curves exhibit shoulder like structures in the region $0.4 \lesssim E_t/W \lesssim 0.7$ and $0.4 \lesssim E_t/W \lesssim 1.0$, respectively, suggesting the formation of the Mott insulating state there.

To clarify these points further, we calculate the density profiles, namely the number of atoms N_i as a function of rescaled distance $r_{SC} = r_i/r_t$, for several fixed values of E_t/W and U/W . We show the results in Fig. 3. Since we adopt a grand canonical ensemble in our calculations, the E_t/W values in Fig. 3 have a small deviation of about ± 0.05 . In Fig. 3(a), at $E_t/W \sim 0.6$, a well developed Mott plateau with $N_i = 1$ from the center to the edge of the cloud appears for large U/W values of 1.5 and 2.0. These plateau profiles are gradually deformed as E_t/W is increased. From Fig. 3(b) and (c), we see that the additional atoms are loaded in the Mott plateau around the center at $E_t/W \sim 0.8$ ($E_t/W \sim 1.0$) when the interaction strength is $U/W = 1.5$ (2.0). In Fig. 3(c) and (d), the Mott plateau is not dominant and is limited to the shell region around $r_{SC} \sim 1$ even for the large interaction $U/W = 2.0$. In all the panels in Fig. 3, for small U/W values of 0.5 and 1.0, there are no Mott plateaus over the entire E_t/W range. This density profile behavior is consistent with the shoulder structure of the R_{SC} curves in Fig. 2.

Our results for the 2D system exhibit good qualitative

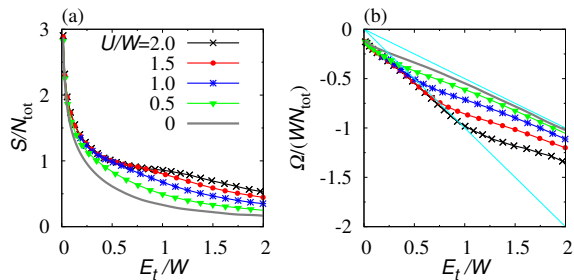


FIG. 4: (Color online) (a) Entropy per atom S/N_{tot} and (b) grand potential per atom Ω/N_{tot} for several values of U/W at $T/W = 0.1$. Thin (light blue) lines in the panel (b) mean $\Omega = -E_t N_{\text{tot}}/2$ and $\Omega = -E_t N_{\text{tot}}$ from top to bottom.

agreement with previous theoretical and experimental results for the 3D system reported in Ref. [12]. This suggests that a proper renormalization allows us to compare the results between two- and three-dimensional optical lattice systems qualitatively.

As a complementary study, we next investigate other thermodynamic quantities at a fixed temperature $T/W = 0.1$. We calculate the entropy per atom S/N_{tot} and the grand potential per atom Ω/N_{tot} as shown in Fig. 4(a) and (b), respectively. Curves of S/N_{tot} reveal a similar E_t/W dependence of R_{SC} to that in Fig. 2. For strongly interacting cases such as $U/W = 1.5$ and 2.0 , the shoulder structure appears in the S/N_{tot} curves around $E_t/W \sim 0.5$, suggesting that the strong correlations induce localized free spins whose entropy takes a constant value of $\ln 2$. It is reasonable to expect that a magnetic ordered phase will appear because these free spins are interacting with each other. However, at $T/W = 0.1$, thermal fluctuations will destroy such an ordered phase, as we discuss in the next section.

Grand potential also provides us with useful information on the Mott transition of the present system. As shown in Fig. 4(b), when $U/W = 1.5$ (2.0), the gradient of Ω/N_{tot} curves gradually changes around $E_t/W \sim 0.75$ (1.0) indicating that there is the crossover between the Mott and metallic phases. Here, the Mott (metallic) phase is defined as the phase in which the Mott insulating (metallic) region is dominant. We find that, in the Mott and metallic phases, the grand potential obeys the relations $\Omega \propto -E_t N_{\text{tot}}$ and $\propto -E_t N_{\text{tot}}/2$, respectively. Note that the characteristic trap energy E_t corresponds to the energy required to add one atom around the edge of the atomic cloud, namely the chemical potential in the limit of zero-tunneling. The difference between these relations, a factor 2, results from the fact that double energy is required to add one atom in the Mott phase.

We now shift our attention to the effects of thermal fluctuations on the quantities shown above. In Fig. 5, we show the temperature dependence of the R_{SC} curves for $U/W = 1.5$. Figure 6 shows the temperature dependence of the density profiles for $U/W = 1.5$ at $E_t/W \sim 0.6$ and 1.0 .

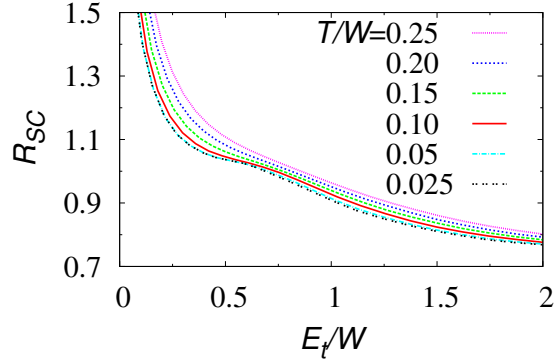


FIG. 5: (Color online) Rescaled cloud size R_{SC} vs E_t/W for different T/W values. The interaction strength is fixed at $U/W = 1.5$.

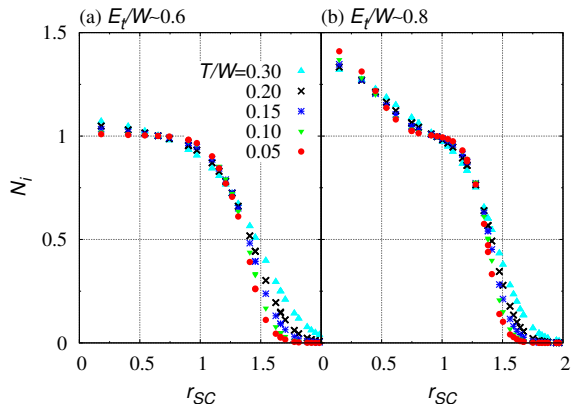


FIG. 6: (Color online) Density profiles of atomic clouds for two characteristic trap energies: (a) $E_t/W \sim 0.6$ and (b) $E_t/W \sim 0.8$. The temperature is varied from $T/W = 0.05$ to $T/W = 0.3$. The interaction strength is fixed at $U/W = 1.5$.

From Fig. 5, we find that, below $T/W = 0.10$, R_{SC} curves have a shoulder structure around $E_t/W \sim 0.5$, and change little as T/W is decreased. On the other hand, above $T/W = 0.10$, thermal fluctuations destroy the shoulder structure; therefore, we find no signature of the Mott insulating state in the R_{SC} curves. However, as shown in Fig. 6, the Mott plateau survives up to $T/W \sim 0.15$, suggesting that the destruction of the shoulder structure of R_{SC} curves is mainly attributed to the thermal excitation of metallic atoms at the edge of the Mott insulating region. Consequently, for $E_t/W \sim 0.6$ and 0.8 , we roughly estimate a specific temperature T^*/W value of ~ 0.15 around which the Mott plateau is destroyed by thermal fluctuations.

We also calculate the entropy per atom S/N_{tot} by varying the temperature as shown in Fig. 7. The S/N_{tot} curves do not saturate at low temperatures ($T/W \lesssim 0.1$) in contrast to those of R_{SC} . At the lowest temperature $T/W = 0.025$ in Fig. 7, the entropy per atom is highly

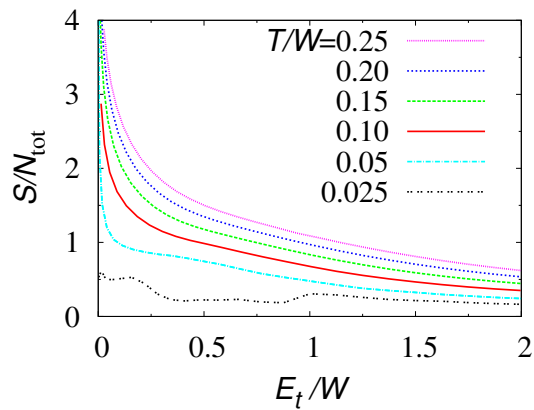


FIG. 7: (Color online) Entropy per atom S/N_{tot} vs E_t/W for several T/W values. The interaction strength is fixed at $U/W = 1.0$.

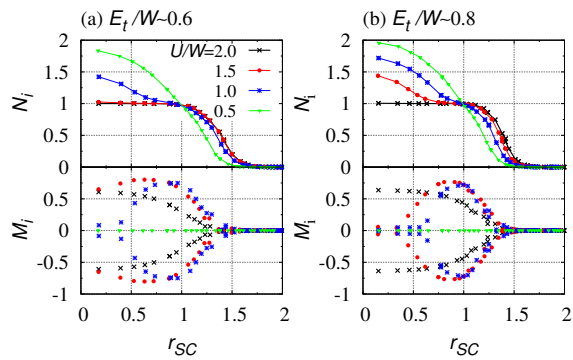


FIG. 8: (Color online) (*top*) the magnetization M_i and (*bottom*) the number of atoms N_i as functions of the rescaled distance r_{SC} for two characteristic trap energies: (a) $E_t/W \sim 0.6$ and (b) $E_t/W \sim 0.8$. The interaction strength is varied from $U/W = 0.5$ to $U/W = 2.0$ and the temperature is fixed at $T/W = 0.025$.

suppressed in the region $0.4 \lesssim E_t/W \lesssim 0.8$. This is due to the fact that a magnetic ordered phase appears at $T/W = 0.025$, as discussed in detail in the next section. We note that entropy is sensitive to magnetic transitions.

As shown in this section, SFA allows us to calculate various thermodynamic quantities at finite temperatures. Such thermodynamic quantities have already been investigated experimentally in ultracold atomic gases trapped in a conventional magnetic trap [37–39]. We hope that these thermodynamic quantities will be measured in optical lattice systems in the near future.

V. MAGNETIC ORDERED PHASE

In the previous section, we showed that entropy shows a characteristic of the AF magnetic transition at a low temperature $T/W = 0.025$. Here, to clarify the properties of the magnetic ordered phase, we investigate the

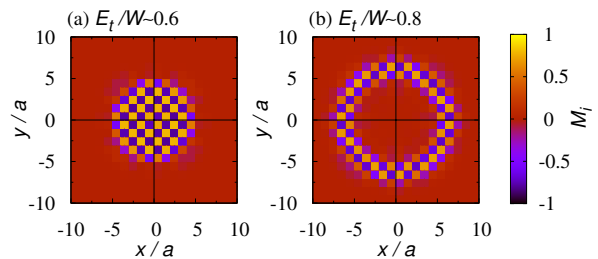


FIG. 9: (Color online) Real-space distribution of the magnetization at $U/W = 1.5$ and $T/W = 0.025$ for (a) $E_t/W \sim 0.6$ and (b) $E_t/W \sim 0.8$.

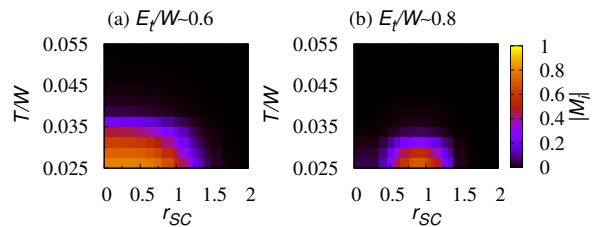


FIG. 10: (Color online) Absolute value of the magnetization $|M_i|$ as a function of r_{SC} and T/W for fixed values of (a) $E_t/W \sim 0.6$ and (b) $E_t/W \sim 0.8$.

present model at a fixed temperature $T/W = 0.025$.

We first look at the magnetization $M_i = \langle n_{i\uparrow} \rangle - \langle n_{i\downarrow} \rangle$. In Fig. 8(a) and (b), we show M_i and N_i as functions of $r_{SC} = r_i/r_t$ for different U/W values at $E_t/W \sim 0.6$ and 0.8 , respectively. Except for a weakly interacting case of $U/W = 0.5$, we find finite values of M_i . The sign of M_i changes alternately from site to site, suggesting the AF order. To clarify this point, we also show the real-space distribution of the magnetization M_i for $U/W = 1.5$ in Fig. 9. We note that the rotational symmetry is broken in the AF ordered region. The magnetization is well-developed in the Mott plateau region. In addition, even in the metallic region in the vicinity of the Mott plateau, the magnetization M_i has a small but finite value [18].

From Figs. 6 and 8, we see that the density profiles of atoms remain unchanged at very low temperatures even though the magnetization M_i becomes finite. As a consequence, the appearance of a magnetic ordered region hardly affects the rescaled cloud size R_{SC} (see also Fig. 5).

The magnetic ordered phase has already been investigated at zero temperature using R-DMFT by M. Snoek *et al.* in Ref. [18]. Our results at very low temperature agree well with their results at zero temperature. We next focus on the temperature dependence of magnetization, and evaluate the critical temperatures of the AF magnetic transition in the present system.

We systematically calculate the magnetization by varying the temperature. Figure 10(a) and (b) show the absolute values of M_i for $U/W = 1.5$ at $E_t/W \sim 0.6$ and

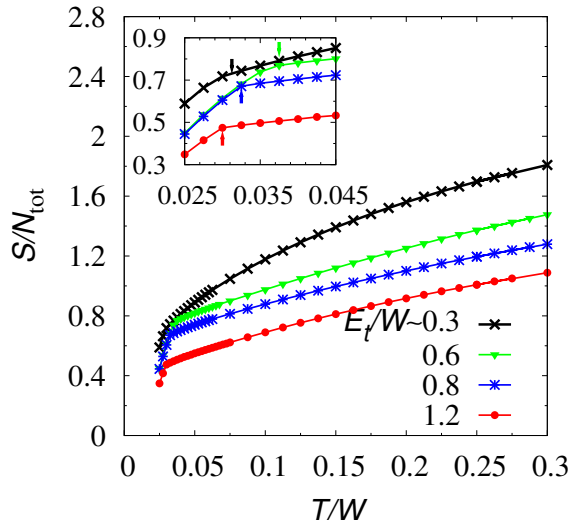


FIG. 11: (Color online) Entropy per atom S/N_{tot} as a function of T/W for several values of E_t/W at $U/W = 1.5$. Inset is an enlarged view and arrows indicate the magnetic transition temperatures.

0.8, respectively. The magnetic ordered region gradually spreads as T/W decreases. Thus we can understand the quantum phase transitions in the present system as follows. The Mott plateau first develops at higher temperatures T^*/W (~ 0.15) (see Fig. 6), and then the magnetic ordered region gradually grows from the inside of the Mott plateau as the temperature decreases below the transition temperature T_c/W (~ 0.04). Note that a well-developed Mott plateau region ($E_t/W \sim 0.6$) has higher transition temperatures than those of the shell-like region ($E_t/W \sim 0.8$).

For a more precise discussion, we calculate the temperature dependence of the entropy per atom. In Fig. 11, we show S/N_{tot} as a function of T/W at $U/W = 1.5$. For $E_t/W \sim 1.2, 0.8, 0.6$ and 0.3 , the S/N_{tot} gradient suddenly becomes steeper at the transition temperatures $T_c/W = 0.029, 0.038, 0.048$ and 0.031 , respectively. In the region from just above the transition temperatures T_c/W to the specific temperatures T^*/W , we find a linear temperature dependence of $S/N_{\text{tot}} \propto T$. Significantly, except for the small E_t/W value of ~ 0.3 , the curves of the entropy per atom show a cusp-like anomaly at T_c/W , suggesting second order magnetic transitions. However, we cannot definitely determine the order of the transition in our present calculation. We reach the conclusion that the transition is of the second or higher order.

Let us discuss this temperature dependence of the entropy per atom in more detail. In a uniform system ($V_t = 0$), the linear temperature dependence of entropy $S \propto T$ is a characteristic of a metallic state, while a constant entropy $S = \ln 2$ is a characteristic of the Mott insulating state at which a localized free spin is induced at each site. On the other hand, in a trapped system

($V_t \neq 0$), both states coexist below T^* , namely the characteristic temperature of a well-developed Mott plateau; therefore, in the region $T_c < T < T^*$, the entropy per atom obeys the relation $S/N_{\text{tot}} = bT + c \ln 2$, where b and c are, roughly speaking, the coefficient depending on the density profiles and the effective mass of atoms. As the temperature is decreased below T^* , free spins in the Mott insulating region interact with each other, and then order antiferromagnetically at $T = T_c$ where the redundant entropy $c \ln 2$ is suddenly released. Above T^* , a complicated temperature dependence can be seen that results from thermal fluctuations of the atoms in the Mott insulating region. Note that the entropy, which is enlarged by strong correlations, and its release play key roles for the magnetic transitions. Therefore, we first observe the developed Mott plateau around T^* , and then find that the magnetic ordered region appears inside this plateau at T_c .

Next, we systematically estimate the AF transition temperatures T_c/W for several choices of $U/W = 1.0, 1.5$ and 2.0 . The results are shown in Fig. 12. In each curve, the transition temperatures as a function of E_t/W have a maximum value around $E_t/W \sim 0.5$ where we see the well-developed Mott plateau. When E_t/W is small, there are insufficient atoms to form a magnetic ordered phase, leading to a very small T_c/W . The long tail of T_c/W curves in the large E_t/W region results from the fact that the shell-like structure of the Mott plateau survives in such regions. For comparison, we calculate T_c^{uni} : the AF transition temperatures for the uniform Hubbard model at half-filling ($V_t = 0$ and $N_{\text{tot}} = L$). We show T_c^{uni}/W for $U/W = 1.0, 1.5$ and 2.0 by the arrows in Fig. 12. With a strongly interacting limit, T_c^{uni} is inversely proportional to U , while for a weakly interacting limit, T_c^{uni} decreases exponentially with decreasing U [40]. Indeed, T_c^{uni}/W has a maximum value around $U/W \sim 1.0$. On the other hand, in the system with a trapping potential, the transition temperatures for $U/W = 1.0$ are comparable to those for $U/W = 1.5$. This is because the Mott plateau does not develop at $U/W = 1.0$, because the effects of the confinement prevail against those of the correlations. For $U/W = 1.5$, we find higher transition temperatures than those for $U/W = 1.0$ and 2.0 over a wide E_t/W range. The results in Fig. 12 suggest that the system for $U/W \sim 1.5$ is more suitable for an observation of the magnetic ordered phase.

Before concluding this section, we compare our present results to other numerical works which have discussed the AF transition temperatures T_c in optical lattice systems without consideration of the effects of the trapping potential [41, 42]. F. Werner *et al.* have estimated $T_c/W \sim 0.04$ at $U/W \sim 1$ [42], and W. Hofstetter *et al.* have done $T_c/W \sim 0.04$ at $U/W = 0.5$ [41]. Our estimated value of $T_c/W \sim 0.04$ around $E_t/W \sim 0.5$ at $U/W = 1$ shows a reasonable agreement with these previous results. We note that, however, lower T_c values are realized except for around $E_t/W \sim 0.5$ in Fig. 12. Furthermore, for a weakly interacting case $U/W = 0.5$, we

cannot find the AF transition down to $T/W = 0.02$ due to the effects of the trapping potential.

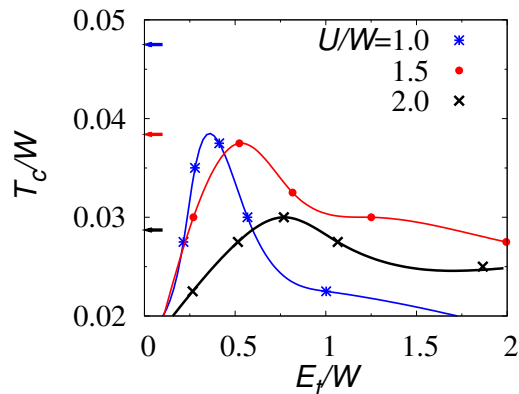


FIG. 12: (Color online) AF transition temperatures T_c/W vs E_t/W for different U/W values. The lines are guides for the eyes. The arrows indicate AF transition temperatures for the uniform Hubbard model at half-filling for $U/W = 1.0, 1.5$ and 2.0 from top to bottom.

VI. SUMMARY

We have investigated the two-component fermionic atoms on a two-dimensional (2D) optical lattice with a harmonic trapping potential at finite temperatures. For a comprehensive understanding of both the Mott transition and the magnetic transition in this system, we have extended the self-energy functional approach (SFA) to deal with inhomogeneous systems. By introducing additional self-consistent loops, a complicated variational problem for an inhomogeneous system following the framework of the SFA is decomposed into several easily solvable SFA problems. We have applied this method to the 2D Hubbard model with a trapping potential. A proper rescaling of the system parameters allows us to qualitatively compare the two-dimensional system with the three-dimensional (3D) one. The calculated results of the rescaled cloud size and density profiles show good qualitative agreement with previous results in Ref. [12]. Furthermore, we have systematically calculated thermodynamic quantities such as entropy and grand potential. We clarified that entropy shows evidence of both the Mott transition and the antiferromagnetic (AF) transition. In addition, we have demonstrated how confinement affects the AF transition temperature. We have estimated the AF transition temperature, and proposed a suitable parameter region for observing the AF ordered phase experimentally.

A direct comparison with experimental results in the 2D optical lattice systems will be useful. The detail information of experimental setups is required for such studies. Additionally, it is very important to investigate d -wave superfluid phase [41]. However, dealing with the

d -wave superfluid correlations is not straightforward in our present choice of the reference system. These issues are beyond our current scope and left as important future works.

Acknowledgments

We thank Y. Takahashi, A. Koga, S. Suga and Y. Tokura for valuable discussions.

Appendix A: Role of the atomic bath

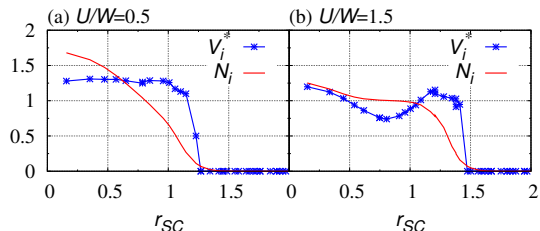


FIG. 13: (Color online) The optimized hybridization V_i^* as a function of r_{SC} for two choices of the interaction strength: (a) $U/W = 0.5$ and (b) $U/W = 1.5$. Other parameters are fixed at $T/W = 0.05$ and $E_t/W \sim 0.8$. For convenience, we also plot the number of atoms N_i .

In this appendix, we comment on the role and importance of the atomic bath with the hybridization $V_{i\sigma}$ in the reference Hamiltonian of Eq. (10).

As mentioned in Sec. III, we adopt the L -sets of two-site Anderson impurity models as the reference system. Here, we explain this procedure in more detail. We first separate a lattice into localized single sites. Then, for each separated site, we additionally introduce the site consisting of non-interacting atoms with the hybridization, and set the energy level of such sites just at Fermi level of the original system. Accordingly, these non-interacting sites are partially occupied and play a role of the atomic reservoir. Furthermore, the hybridization in the reference Hamiltonian corresponds to the hopping in the original Hamiltonian.

It is known that, when the interaction strength is increasing, an effective energy scale of the hopping becomes much smaller. In other words, the renormalization effects are induced by the effects of correlations. We will demonstrate that the hybridization $V_{i\sigma}$ in the reference Hamiltonian clearly reflects such many-body dynamics via the variational condition $\partial\Omega/\partial V_{i\sigma} = 0$. In Fig. 13, we plot the optimized values of the hybridization $V_{i\sigma}^*$ which satisfy all of the required conditions mentioned in Sec. III. Figure 13(a) and (b) show $V_i^* \equiv V_{i\uparrow}^* = V_{i\downarrow}^*$ as a function of r_{SC} for $U/W = 0.5$ and 1.5 , respectively. We set other parameters as $T/W = 0.05$ and $E_t/W \sim 0.8$. In Fig. 13(a), we see large and constant V_i values in an

occupied region ($r_{SC} \lesssim 1.3$). Note that, we reasonably choose $V_i = 0$ in an unoccupied region ($r_{SC} \gtrsim 1.3$) since the variational conditions $\partial\Omega/\partial V_{i\sigma} = 0$ is satisfied by

any values of $V_{i\sigma}$. On the other hand, in Fig. 13(b), we see that values of V_i decrease in the Mott plateau region ($0.5 < r_{SC} < 1$), indicating the renormalization effects.

-
- [1] Q. Chen, J. Stajic, S. Tan, and K. Levin, *Phys. Rep.* **412**, 1 (2005).
- [2] C. A. Regal, M. Greiner, and D. S. Jin, *Phys. Rev. Lett.* **92**, 040403 (2004).
- [3] I. Bloch, *Nat. Phys.* **1**, 23 (2005).
- [4] M. Greiner and S. Fölling, *Nature* **453**, 1 (2008).
- [5] G.-B. Jo, Y.-R. Lee, J.-H. Choi, C. A. Christensen, T. H. Kim, J. H. Thywissen, D. E. Pritchard, and W. Ketterle, *Science* **325**, 1521 (2009).
- [6] D. Jaksch, C. Bruder, J. I. Cirac, C. W. Gardiner, and P. Zoller, *Phys. Rev. Lett.* **81**, 3108 (1998).
- [7] W. Zwerger, *Journal of Optics B: Quantum and Semi-classical Optics* **5**, S9 (2003).
- [8] D. Jaksch and P. Zoller, *Annals of Physics* **315**, 52 (2005).
- [9] M. Greiner, O. Mandel, T. Esslinger, T. W. Hansch, and I. Bloch, *Nature* **415**, 39 (2002).
- [10] M. Köhl, H. Moritz, T. Stöferle, K. Günter, and T. Esslinger, *Phys. Rev. Lett.* **94**, 080403 (2005).
- [11] R. Jördens, N. Strohmaier, K. Günter, H. Moritz, and T. Esslinger, *Nature* **455**, 204 (2008).
- [12] U. Schneider, L. Hackermüller, S. Will, T. Best, I. Bloch, T. A. Costi, R. W. Helmes, D. Rasch, and A. Rosch, *Science* **322**, 1520 (2008).
- [13] N. Gemelke, X. Zhang, C.-L. Hung, and C. Chin, *Nature* **460**, 995 (2009).
- [14] T. Fukuhara, Y. Takasu, M. Kumakura, and Y. Takahashi, *Phys. Rev. Lett.* **98**, 030401 (2007).
- [15] T. Fukuhara, S. Sugawa, M. Sugimoto, S. Taie, and Y. Takahashi, *Phys. Rev. A* **79**, 041604(R) (2009).
- [16] P. A. Lee, N. Nagaosa, and X.-G. Wen, *Rev. Mod. Phys.* **78**, 17 (2006).
- [17] R. W. Helmes, T. A. Costi, and A. Rosch, *Phys. Rev. Lett.* **100**, 056403 (2008).
- [18] M. Snoek, I. Titvinidze, C. Töke, K. Byczuk, and W. Hofstetter, *New Journal of Physics* **10**, 093008 (2008).
- [19] A. Koga, T. Higashiyama, K. Inaba, S. Suga, and N. Kawakami, *J. Phys. Soc. Jpn.* **77**, 073602 (2008).
- [20] A. Koga, T. Higashiyama, K. Inaba, S. Suga, and N. Kawakami, *Phys. Rev. A* **79**, 013607 (2009).
- [21] M. Potthoff, *Eur. Phys. J. B* **32**, 429 (2003).
- [22] M. Potthoff, *Eur. Phys. J. B* **36**, 335 (2003).
- [23] M. Potthoff, M. Aichhorn, and C. Dahnken, *Phys. Rev. Lett.* **91**, 206402 (2003).
- [24] M. Balzer, B. Kyung, D. Senechal, A.-M. S. Tremblay, and M. Potthoff, *EPL (Europhysics Letters)* **85**, 17002 (2009).
- [25] J. M. Luttinger and J. C. Ward, *Phys. Rev.* **118**, 1417 (1960).
- [26] C. Dahnken, M. Aichhorn, W. Hanke, E. Arrigoni, and M. Potthoff, *Phys. Rev. B* **70**, 245110 (2004).
- [27] M. Balzer, W. Hanke, and M. Potthoff, *Phys. Rev. B* **77**, 045133 (2008).
- [28] K. Inaba and S.-i. Suga, *Phys. Rev. A* **80**, 041602(R) (2009).
- [29] A. Rapp, G. Zarand, C. Honerkamp, and W. Hofstetter, *Phys. Rev. Lett.* **98**, 160405 (2007).
- [30] F. Wilczek, *Nat. Phys.* **3**, 375 (2007).
- [31] R. W. Cherng, G. Refael, and E. Demler, *Phys. Rev. Lett.* **99**, 130406 (2007).
- [32] M. A. Cazalilla, A. F. Ho, and M. Ueda, *New Journal of Physics* **11**, 103033 (2009).
- [33] T. B. Ottenstein, T. Lompe, M. Kohnen, A. N. Wenz, and S. Jochim, *Phys. Rev. Lett.* **101**, 203202 (2008).
- [34] J. H. Huckans, J. R. Williams, E. L. Hazlett, R. W. Stites, and K. M. O'Hara, *Phys. Rev. Lett.* **102**, 165302 (2009).
- [35] J. Ortloff, M. Balzer, and M. Potthoff, *Eur. Phys. J. B* **58**, 37 (2007).
- [36] J. T. Stewart, J. P. Gaebler, and D. S. Jin, *Nature* **454**, 744 (2008).
- [37] J. R. Ensher, D. S. Jin, M. R. Matthews, C. E. Wieman, and E. A. Cornell, *Phys. Rev. Lett.* **77**, 4984 (1996).
- [38] M.-O. Mewes, M. R. Andrews, N. J. van Druten, D. M. Kurn, D. S. Durfee, and W. Ketterle, *Phys. Rev. Lett.* **77**, 416 (1996).
- [39] D. Jin, J. Ensher, M. Matthews, C. Wieman, and E. Cornell, *Czech. J. Phys.* **46**, 3070 (1996).
- [40] M. Jarrell, *Phys. Rev. Lett.* **69**, 168 (1992).
- [41] W. Hofstetter, J. I. Cirac, P. Zoller, E. Demler, and M. D. Lukin, *Phys. Rev. Lett.* **89**, 220407 (2002).
- [42] F. Werner, O. Parcollet, A. Georges, and S. R. Hassan, *Phys. Rev. Lett.* **95**, 056401 (2005).